Direct intracellular visualization of Ebola virus-receptor interaction by *in situ* proximity ligation

Eva Mittler [a], Tanwee P Alkutkar [a,*], Rohit K Jangra [a], and Kartik Chandran [a,#]

[a] Albert Einstein College of Medicine, Department of Microbiology & Immunology, Bronx, New York, USA

Running head: Delineating EBOV GP-NPC1 binding by proximity ligation

[#] Address correspondence to Kartik Chandran, kartik.chandran@einsteinmed.org

* Present address: Department of Integrative Structural and Computational Biology, The Scripps Research Institute, La Jolla, California, USA

Word count - abstract: 250

Word count - text: 3945

ABSTRACT

Ebola virus (EBOV) entry into host cells comprises stepwise and extensive interactions of the sole viral surface glycoprotein GP with multiple host factors. During the intricate process, following virus uptake and trafficking to late endosomal/lysosomal compartments, GP is proteolytically processed to GP_{CL} by the endosomal proteases cathepsin B and L unmasking GP's receptor-binding site. Engagement of GP_{CL} with the universal filoviral intracellular receptor Niemann-Pick C1 (NPC1) eventually culminates in fusion between viral and cellular membranes, cytoplasmic escape of the viral nucleocapsid and subsequent infection. Mechanistic delineation of the indispensable GP_{CL}:NPC1 binding step has been severely hampered by the unavailability of a robust cell-based assay assessing interaction of GP_{CL} with full-length endosomal NPC1.

Here, we describe a novel *in situ* assay to monitor GP_{CL}:NPC1 engagement in intact, infected cells. Visualization of the subcellular localization of binding complexes is based on the principle of DNA-assisted, antibody-mediated proximity ligation. Virus-receptor binding monitored by proximity ligation was contingent on GP's proteolytic cleavage, and was sensitive to perturbations in the GP_{CL}:NPC1 interface. Our assay also specifically decoupled detection of virus-receptor binding from steps post-receptor binding, such as membrane fusion and infection. Testing of multiple FDA-approved small molecule inhibitors revealed that drug treatments inhibited virus entry and GP_{CL}:NPC1 recognition by distinctive mechanisms. Together, here we present a newly established proximity ligation assay, which will allow us to dissect cellular and viral requirements for

46 filovirus-receptor binding, and to delineate the mechanisms of action of inhibitors on
47 filovirus entry in a cell-based system.
48
49 **IMPORTANCE**
50
51 Ebola virus causes episodic but increasingly frequent outbreaks of severe disease in
52 Middle Africa, as shown by a currently ongoing outbreak in the Democratic Republic of
53 Congo. Despite considerable effort, FDA-approved anti-filoviral therapeutics or targeted
54 interventions are not available yet. Virus host-cell invasion represents an attractive target
55 for antivirals; however our understanding of the inhibitory mechanisms of novel
56 therapeutics is often hampered by fragmented knowledge of the filovirus-host molecular
57 interactions required for viral infection. To help close this critical knowledge gap, here,
58 we report an *in situ* assay to monitor binding of the EBOV glycoprotein to its receptor
59 NPC1 in intact, infected cells. We demonstrate that our *in situ* assay based on proximity
60 ligation represents a powerful tool to delineate receptor-viral glycoprotein interactions.
61 Similar assays can be utilized to examine receptor interactions of diverse viral surface
62 proteins whose studies have been hampered until now by the lack of robust *in situ*
63 assays.
64

INTRODUCTION

Members of the family *Filoviridae*, including Ebola virus (EBOV), are emerging zoonotic pathogens that cause episodic but increasingly frequent outbreaks of a highly lethal disease in Middle Africa (1). Along with the big EBOV outbreak of 2014-16 in West Africa, the ongoing outbreak of EBOV disease in the Democratic Republic of Congo, the second largest outbreak on record with >3,400 confirmed cases and >2,200 deaths (as of April 2020) and spill-over cases to neighboring Uganda highlight the potential of filoviruses to cause health emergencies of international scope (2). There is an urgent need for effective countermeasures; however, their development is hindered by our limited understanding of filovirus-host molecular interactions required for viral entry and infection.

The single filovirus-encoded spike glycoprotein (GP) is necessary and sufficient to mediate all steps in viral entry into host cells, culminating in cytoplasmic escape of the viral nucleocapsid. Following endocytosis, virions traffic to late endosomes/lysosomes (LE/LY) (3–6), where GP gains access to multiple essential host factors. GP is proteolytically processed by endosomal cysteine cathepsins B and L (CatB and CatL, respectively), which remove the heavily glycosylated C–terminal glycan cap and mucin domain sequences in the GP_1 subunit (7–9), thereby exposing a recessed receptor-binding site (RBS). This cleaved GP species (GP_{CL}) binds domain C of Niemann-Pick C1 (NPC1), an ubiquitously expressed cholesterol transporter embedded in endo/lysosomal membranes that acts as an universal intracellular receptor for all filoviruses (10–14). Although GP_{CL}:NPC1 recognition is a prerequisite for downstream steps in virus entry and infection, *in vitro* work suggests that NPC1 binding is not

sufficient to trigger large-scale conformational changes in GP or to initiate a subsequent merger of viral and host membranes (15, 16). Indeed, NPC1's precise role beyond GP binding, which presumably provides a physical link between virus particles and host membranes, remains elusive to date.

Because a robust cell-based assay assessing the interaction of GP_{CL} with full-length endosomal NPC1 in its native context has been unavailable, mechanistic studies of this indispensable virus-receptor interaction have been largely limited to *in vitro* assays. These assays are predominantly based on a truncated, soluble form of a single domain in NPC1, domain C, as well as on *in vitro*-cleaved GPs (11, 12). However, studies with NPC1-targeting inhibitors suggest that these assays do not fully recapitulate the authentic interaction(s) between *in situ*-cleaved GP and full-length NPC1 in its membrane context within late endosomes and/or lysosomes (16). To address this gap, we describe herein an *in situ* assay to monitor GP_{CL}:NPC1 binding in individual endosomal compartments of intact, infected cells by using DNA-guided, antibody-mediated proximity ligation. We employed this assay to show that GP_{CL}:NPC1 interaction is restricted to the lumina of $NPC1^+$ LE/LY, is contingent on the proteolytic cleavage of GP and is sensitive to the mutational disruption of the GP_{CL}:NPC1 interface. Testing of multiple FDA-approved small molecule inhibitors in our assay revealed that drug treatments inhibited virus entry and GP_{CL}:NPC1 recognition by distinct mechanisms. Application of this assay will allow us to dissect the cellular and viral requirements for filovirus-receptor interaction, and to delineate the mechanisms of action of small molecule inhibitors on filovirus entry.

RESULTS

Development of an assay visualizing EBOV GP:NPC1 binding in intact cells by *in situ* proximity ligation

During viral entry, proteolytically cleaved forms of EBOV GP (GP_{CL}) interact with their critical endosomal receptor NPC1. We postulated that an *in situ* proximity ligation assay (PLA) could be used to monitor this essential binding step in intact cells. To detect viral particles, we used a recombinant vesicular stomatitis virus (rVSV) containing the viral phosphoprotein P linked to a fluorescent monomeric NeonGreen (mNG-P) protein, and bearing EBOV GP (17). Viral particles were allowed to attach at 4°C to U2OS human osteosarcoma cells stably expressing NPC1 tagged with a blue fluorophore, eBFP2 (17), and the cells were then shifted to 37°C to allow synchronized viral internalization. Visualization of fixed $U2OS^{NPC1\text{-}eBFP2}$ cells by fluorescence microscopy revealed that most internalized viral particles reached NPC1-containing late endosomes ($NPC1^+$ LE) within 60 min (Fig. 1).

To detect closely apposed GP_{CL} and NPC1 molecules in infected cells, we incubated them with oligonucleotide-linked monoclonal antibodies directed against each protein: GP's highly conserved receptor-binding site (RBS), unmasked by proteolytic cleavage to GP_{CL} in endosomes, was detected with the RBS-specific antibody MR72 (17–19), and NPC1 was detected with the domain C-specific antibody mAb-548 (17). Circular DNA molecules were generated by oligonucleotide-guided proximity ligation, amplified *in situ* and visualized with a fluorophore-conjugated detector oligonucleotide (20, 21). PLA signal required the addition of both, MR72 and mAb-548

antibodies, and was only observed in cells that were allowed to internalize viral particles (Fig. S1). Also, PLA signal colocalized with VSV mNG-P particles bearing EBOV GP in the lumina of NPC1$^+$ LE (Fig. 1A). Proximity ligation and viral trafficking to NPC1$^+$ LE displayed similar kinetics—both peaked within 60 min post-viral uptake, followed by a plateau phase (Figs. 1A and B). Although most internalized viral particles trafficked to and colocalized with NPC1$^+$ compartments (Fig. 1B), only a subset of these VSV$^+$/NPC1$^+$ vesicles also displayed PLA signal (Fig. 1B). Accordingly, in the following studies aimed at determining the viral and cellular requirements for proximity-dependent ligation of GP_{CL}- and NPC1-specific antibodies, we routinely enumerated the number of VSV$^+$/NPC1$^+$ compartments per cell, and reported the percentage of these compartments that were also positive for PLA signal (VSV$^+$/NPC1$^+$/PLA$^+$).

Proximity ligation is sensitive to perturbations in the GP_{CL}:NPC1 domain C interface

Specific interactions of EBOV GP with NPC1 domain C have been mapped to amino acid residues in the GP_1 subunit that are exposed upon proteolytic cleavage (11, 18, 22). Mutations of the charged surface-exposed amino acids K114/K115 and the polar amino acid T83 led to significant defects in NPC1 binding and viral entry (5, 18). To determine if these mutations impact proximity ligation, we exposed cells to VSVs bearing $GP^{T83M/K114E/K115E}$. Virions were efficiently trafficked to NPC1$^+$ LE and underwent GP_1 cleavage, as indicated by detection of the GP_1 RBS with the mAb MR72. However, viral infectivity was greatly diminished (Figs. S2A and S2B). Concordantly, we observed significant reduction of VSV$^+$/NPC1$^+$/PLA$^+$ colocalization, suggesting that GP_{CL}:NPC1 engagement in LE is necessary for PLA signal formation (Fig. 2A).

The small molecule filovirus entry inhibitor 3.47 was described to block EBOV GP-dependent entry and infection potentially by interfering with GP_{CL}:NPC1 recognition (12). Accordingly, we directly compared the effect of 3.47 on viral entry in wild-type U2OS cells expressing basal levels of NPC1 against that in $U2OS^{NPC1\text{-}eBFP2}$ cells used for the PLA (Fig. 2C). Consistent with its activity as an NPC1-targeting inhibitor, and as shown previously, 3.47's antiviral activity was substantially attenuated in cells over-expressing NPC1, but we were nevertheless able to identify a concentration (1 μM) that afforded ~50% inhibition of viral entry; higher concentrations of 3.47 were cytotoxic. Pre-treatment of $U2OS^{NPC1\text{-}eBFP2}$ cells with 3.47 at 1 μM significantly reduced PLA signal (Fig. 2B) but did not modify $NPC1^{+}$ LE morphology, block viral trafficking and GP cleavage, or influence detection by the assay antibodies, MR72 and mAb-548 (Fig. S2C). Our data that both genetic and pharmacological disruptions of the virus-receptor interface inhibit PLA strongly suggests that this assay indeed monitors GP_{CL}:NPC1 domain C engagement in endosomal compartments.

Detection of GP_{CL}:NPC1 binding by PLA requires endosomal cleavage of GP

Endosomal host cysteine cathepsins B and L (CatB and CatL, respectively) are key mediators of the entry-related GP→GPCL cleavage that is required for GPCL:NPC1 binding and viral membrane fusion (5, 7–9). Their inactivation by pan-cysteine cathepsin inhibitors, including E-64 and E-64d, blocks filovirus entry ((7, 8); also see Fig. S3A). Concordantly, we found that pre-treatment of cells with E-64d abolished both GP cleavage (and consequently exposure of the GP_1 NPC1-binding site recognized by MR72; Fig. 3B) and GP_{CL}:NPC1 engagement as measured by PLA (Fig. 3A). Intriguingly,

179 previous work has also hinted at the existence of cellular target(s) of E-64 in addition to
180 CatB and CatL, whose inhibition imposes one or more blocks to viral entry (7, 8, 23, 24).
181 To further investigate the cysteine protease-dependent EBOV entry mechanism, we
182 generated *CatB/L*-knockout (KO) U2OS cell lines by CRISPR/Cas9 genome engineering
183 (Fig. S4A). As expected, the *CatB/L*-KO cells lacked CatB and CatL activity and were
184 substantially resistant to EBOV GP-dependent entry (Fig. S4B and C). Surprisingly,
185 however, and in contrast to our findings in E-64d treated cells, viral particles underwent
186 efficient exposure of the NPC1-binding site (and MR72 epitope) in GP in *CatB/L*-KO cells
187 (Fig. 3B). Despite this apparent capacity for GP cleavage in the absence of CatB and
188 CatL, viral particles were nevertheless unable to engage NPC1 as measured by PLA (Fig.
189 3A).

190 GP priming in viral entry can be recapitulated *in vitro* by incubating rVSV bearing
191 full-length EBOV GP with CatL or the bacterial protease thermolysin (THL) which mimics
192 CatL/B cleavage (8); both cleave off GP_1 sequences corresponding to the glycan cap
193 and mucin domain. Increased infectivity of viral particles bearing THL/CatL-cleaved GPs
194 was reported previously, and can be attributed to improved cell binding of virions as well
195 as increased accessibility of the GP's RBS for NPC1 domain C interaction ((7, 11, 25);
196 also see Fig. S3B). *In vitro* cleavage of GP significantly enhanced GP_{CL}:NPC1 domain C
197 binding *in situ* by 1.5- to 2-fold indicating that proteolytic processing of GP is
198 indispensable for detection of virus-receptor interaction by proximity ligation (Fig. 3C).
199 In order to determine possible requirements for additional cysteine protease activity pre
200 NPC1-binding, we evaluated proximity ligation with THL-cleaved GP in the presence of
201 the pan-cysteine cathepsin inhibitor E-64d. Here, the absence of cysteine protease

proteolytic activity did not affect GP_{CL}:NPC1 engagement (Fig. 3D), suggesting the existence of an E-64d-sensitive downstream entry block post-NPC1 binding, as previously proposed (5, 23).

In situ proximity ligation decouples GP_{CL}:NPC1 interaction from post-binding entry steps

As one of the critical steps in viral entry, GP:NPC1 interaction is the starting point for subsequent post-binding entry processes including, among others, membrane fusion triggering, cytoplasmic nucleocapsid escape and infection (5, 10–12). To examine if the established *in situ* PLA selectively monitored GP_{CL}:NPC1 engagement or, in addition, also downstream steps such as membrane fusion, we made use of an EBOV GP mutant harboring amino acid substitutions in the GP_1 internal fusion loop, $GP^{L529A/I544A}$. Amino acids L529 and I544 were shown to form a fusogenic hydrophobic surface at the tip of the fusion loop and proposed to be crucial for insertion of the loop into host membranes and subsequent membrane fusion steps (26, 27). Late-endosomal delivery of VSV bearing $GP^{L529A/I544A}$ and exposure of GP's RBS did not differ substantially from those of VSV harboring wild-type GP. However, steps post NPC1-binding, including membrane fusion triggering and virus infection were inhibited ((5); also see Fig. S5A). Consistent with these observations, *in situ* proximity ligation of VSV bearing $GP^{L529A/I544A}$ resembled that obtained with VSV decorated with wild-type GP (Fig. 4A).

Previous work identified a variety of antibodies with neutralizing activity against EBOV. Those displaying exceptional neutralizing potency were described to target conformational epitopes located in the base subdomain of the GP trimeric complex (28–

32). It was proposed that these base-binding antibodies efficiently block fusogenic rearrangements of GP, thereby inhibiting viral entry steps downstream of NPC1 binding. We used these neutralizing antibodies to further investigate if *in situ* PLA monitored GP_{CL}:NPC1 binding specifically or also integrated post-receptor binding events (e.g., viral membrane fusion). We tested antibodies targeting the GP_1-GP_2 interface (KZ52, mAb100), the GP_1-GP_2 interface plus the glycan cap (ADI-15946), or a subdomain of the fusion loop, the heptad repeat 2 (ADI-16061). Pre-incubation of VSVs with these neutralizing antibodies (50 μg/mL) afforded delivery of virus:antibody complexes to $NPC1^+$ LE, but did not hinder virus trafficking to LEs itself or proteolytic processing to GP_{CL} (Fig. 4B, right panel and Fig. S5B-C). However, infection was blocked under these conditions, as expected (Fig. 4B, left panel). Despite their potent neutralizing activity, and consistent with the specified target epitopes as well as previously reported *in vitro* NPC1-binding studies (28–32), base-binding antibodies mAb100 and ADI-15946 had little or no effect on *in situ* PLA, consistent with our hypothesis that this assay selectively detects GP_{CL}:NPC1 complex formation (Fig. 4C). Surprisingly, incubation with KZ52 and ADI-16061 slightly improved PLA signal, possibly because they enhanced an upstream step: the delivery of VSV bearing GP_{CL} to $NPC1^+$ LE (Fig. 4C).

Collectively, our results provide strong evidence that the *in situ* PLA specifically monitors GP_{CL}:NPC1 binding in infected cells and decouples the detection of virus-receptor binding from post-receptor binding steps in viral entry.

246 **Small molecule inhibitor-mediated selective interference of GP:NPC1 binding**
247 **delineated by *in situ* PLA**

248 The unprecedented EBOV outbreak in West Africa 2013-16 uncovered a pressing need
249 for anti-EBOV therapeutics; since then, numerous studies screened for and
250 characterized FDA-approved drugs with anti-filoviral activity. The most promising drug
251 candidates, amiodarone, bepridil, clomifene, sertraline, and toremifene were reported to
252 block one or several steps during EBOV entry (16, 33–38). As their precise mechanisms
253 of anti-EBOV activity still remain elusive, we examined the capacity of these inhibitors to
254 alter intracellular GP_{CL}:NPC1 interaction in the PLA. As a control, we also tested the well
255 characterized amphiphilic drug U18666A, which was described to block cholesterol
256 export from lysosomes and shown to inhibit EBOV entry at higher concentrations, but
257 not to impact GP_{CL}:NPC1 binding *in vitro* (10, 16, 39).

258 We first titrated the drugs in an EBOV entry assay in wild-type U2OS and
259 $U2OS^{NPC1\text{-}eBFP2}$ cells over-expressing NPC1 employed in the PLA (Fig. 5A). Several of the
260 inhibitors were less potent in NPC1-overexpressing cells than in wild-type cells, as
261 reported previously, suggesting they act via the GP_{CL}:NPC1 axis ((16); also see Fig. S6A).
262 Some inhibitors hampered VSV trafficking to $NPC1^+$ LE, whereas others had little or no
263 effect on viral delivery to $NPC1^+$ LE compared to a DMSO-treated control (Fig. S6B).
264 Because these trafficking defects likely contribute to the observed inhibition in infection,
265 we sought to discount these trafficking effects on GP_{CL}:NPC1 binding by focusing
266 exclusively on PLA activity in $VSV^+/NPC1^+$ compartments. Importantly, these inhibitors
267 exhibited little or no effect on GP cleavage (detected by MR72) or the accessibility of
268 NPC1 domain C (detected by mAb-548; Fig. 5C and Fig. S6C).

Screening the inhibitory agents via PLA revealed that amiodarone, bepridil, clomifene, sertraline, and toremifene all significantly interfered with GP_{CL}:NPC1 interaction as compared to a DMSO-treated control (Fig. 5B). By contrast, but consistent with previous *in vitro* data, U18666A did not block GP_{CL}:NPC1 binding (Fig. 5B). The drug treatments also substantially modified NPC1 trafficking to LE and/or LE localization: we observed pronounced imbalances in NPC1 distribution, illustrated by LE vesicles with extensively elevated or decreased NPC1 levels accumulating in the perinuclear regions of cells (Fig. 5C and S6C). Further, NPC1's transporter activity was strongly impaired: although cells did not exhibit cholesterol accumulation in $NPC1^+$ LE following the short-term drug treatments carried out prior to PLA measurements, prolonged inhibitor incubations (16 h instead of 1 h incubation prior to PLA) clearly blocked cholesterol clearance from LE (Fig. 5C and Fig. S6C, upper panel).

In summary, our results imply that a number of FDA-approved small molecule inhibitors interfere with GP_{CL}:NPC1 engagement, and such block downstream viral entry steps. However, our findings and previously published work indicate that the inhibitory mode of action of these compounds is likely multifactorial. Although our data suggests that some of the compounds directly affect GP_{CL}:NPC1 interaction in endosomal compartments during entry, they also uncover contributions from drug-induced changes in the morphology and distribution of $NPC1^+$ compartments.

DISCUSSION

Interaction of the filovirus spike protein GP with its universal intracellular receptor NPC1 is indispensable for viral entry and infection (10–14). However, our understanding of the mechanism of GP:NPC1 recognition is largely derived from *in vitro* assays that use detergent-extracted NPC1 or a soluble form of the GP-interacting domain C of NPC1 and *in vitro*-cleaved GP_{CL} (11, 12). Although powerful, these assays likely do not fully recapitulate the authentic virus-receptor interaction in late endo/lysosomal compartments. As a case in point, a number of small molecule entry inhibitors that appear to target NPC1 in cells do not block GP_{CL}:NPC1 domain C interaction *in vitro*, leaving questions about their mechanism of action open (16).

Here, we describe a novel assay that monitors the GP:NPC1 interaction in intact cells. Detection of the virus-receptor complexes *in situ* is based on the principle of DNA-assisted, antibody-mediated proximity ligation (20, 21). Several studies have used PLAs to detect interaction of viruses with host proteins at the plasma membrane (40), in the cytoplasm (41, 42) and early endosomes (43). To our knowledge, our assay represents the first example to afford visualization of protein-protein interactions in late endosomal/lysosomal compartments.

Previous studies used *in vitro* protease treatments in conjunction with infectivity measurements in protease inhibitor-treated or genetically engineered cells to establish a requirement for GP cleavage in EBOV entry (7–9). Further, *in vitro* binding studies with soluble NPC1 domains demonstrated that GP cleavage is required for virus-receptor interaction (10–14). Here, we used the PLA to directly investigate the role of GP

proteolytic cleavage in GP:NPC1 interaction within cellular endo/lysosomal compartments. Concordant with our current understanding, we found that blockade of all endosomal cysteine cathepsins with the pan-cysteine cathepsin inhibitor E-64d abrogated both GP cleavage and GP:NPC1 association *in situ* and that *in vitro* pre-cleavage of EBOV GP to GP_{CL} significantly boosted this interaction. We also observed that genetic knockout of the two key cysteine cathepsins identified previously—CatB and CatL—substantially inhibited GP:NPC1 association as measured by PLA. Unexpectedly, knocking out *CatB* and *CatL* did not prevent exposure of the RBS in endosomes, as judged by the continued capacity of RBS-specific mAb MR72 to detect viral particles. Thus, one or more non-CatB/CatL cysteine cathepsins appear to at least partially cleave GP in endosomes in a manner that, however, does not permit stable GP:NPC1 association. Alternatively, it is possible, at least in principle, that CatB and/or CatL mediate additional yet undiscovered cleavage events that are required for GP:NPC1 binding.

Similar to published *in vitro* GP:NPC1 binding assays, our *in situ* PLA also specifically monitored GP:NPC1 interactions decoupling them from downstream post-binding steps allowing us to entirely focus on molecular mechanisms underlying the indispensable receptor binding. We employed fusion-blocking GP mutants and neutralizing antibodies targeting epitopes essential for GP's conformational rearrangements during membrane fusion; both interventions however left GP_{CL}:NPC1 binding measured by PLA largely unaffected. Previous publications suggested a dual mechanism of action for several of these antibodies, KZ52, mAb100, and ADI-15946 (28, 30); to block EBOV GP-mediated infection they hampered post-NPC1-binding steps,

335 and interfered with GP's proteolytic processing *in vitro*. Surprisingly, the latter *in vitro*
336 findings were not recapitulated by the *in situ* PLA. Our results suggest that in the
337 presence of neutralizing antibodies the Cat B/L cleavage sites located in GP's β13-14
338 loop were readily accessible in an *in situ* endosomal environment while they did not
339 appear to be in the *in vitro* cell-free system. While the RBS-specific mAb MR72 does not
340 allow to monitor minor changes in GP cleavage efficiency, our PLA results indicate
341 sufficient cleavage to allow efficient NPC1 binding. Further, our experiments suggest
342 that *in vitro* cleavage studies do not adequately recapitulate the authentic interactions
343 within the trifecta of endosomal proteases, virus glycoproteins and GP-targeting mAbs
344 in an acidic endosomal environment.

345 Lastly, by examining the effect of small molecule inhibitors on GP_{CL}:NPC1 binding,
346 we further unraveled their multifaceted mechanisms of inhibitory action towards EBOV
347 GP-mediated infection. All FDA-approved drugs tested, amiodarone, bepridil, clomifene,
348 sertraline, and toremifene, significantly hampered GP_{CL}:NPC1 interaction measured by
349 *in situ* PLA. Previous reports focused on bepridil, sertraline and toremifene destabilizing
350 the GP's prefusion conformation by binding to a cavity at the interface of GP_1 and GP_2
351 *in silico* (35, 38). Our data also indicated striking changes in the intracellular distribution
352 and morphology of $NPC1^+$ LE/LY, as well as NPC1's cholesterol transporter function
353 which was most notable for toremifene, clomifene, and sertraline suggesting they (in
354 addition) also acted via the GP_{CL}:NPC1 axis; overexpression of NPC1 clearly
355 counteracted their inhibitory mechanism during infection. We propose that the loss of
356 GP_{CL}:NPC1 binding is most likely caused by adverse effects on both, NPC1 and GP,
357 leading to destabilization of GP and drastic modifications in the $NPC1^+$ LE/LY phenotype.

Resolving the effects of small molecule inhibitors on GP_{CL}:NPC1 binding remains the focus of ongoing work and will help us to decode this interaction in more detail.

In summary, the newly established *in situ* proximity ligation assay represents a powerful tool to delineate molecular mechanisms underlying receptor-filoviral glycoprotein interactions, to characterize host factors modulating EBOV entry, and to unravel the mode of action of antibodies and small molecule inhibitors in a cell-based system. Our data indicates that *in vitro* and *in silico* studies, while informative, have severe limitations in adequately recapitulating authentic receptor-glycoprotein interactions in host cells. Hence, we propose to modify and translate the employed *in situ* assay to unravel the receptor interactions of diverse viral surface proteins.

MATERIAL AND METHODS

Cells and viruses. Human osteosarcoma U2OS cells were cultured in modified McCoy's 5A medium (Life Technologies) supplemented with 10% fetal bovine serum (Atlanta Biologicals), 1% penicillin-streptomycin (Life Technologies), and 1% GlutaMax (Life Technologies). Cells were kept at 37°C with 5% CO_2 in a humidified incubator. U2OS cells stably overexpressing NPC1-eBFP2 were generated as described previously and maintained under the same conditions mentioned above (17). Propagation of recombinant vesicular stomatitis Indiana virus (rVSV) expressing eGFP in the first position and bearing the VSV G or EBOV GP glycoprotein, derived from EBOV/H.sap/COD/76/Yam-Mayinga (EBOV “Mayinga” isolate) as well as an rVSV

bearing the EBOV GP glycoprotein, and an mNeongreen-phosphoprotein P (mNG-P) fusion protein has been described previously (5, 44–46). Pseudotyped VSVs bearing mNG-P and variant GPs, $GP^{T83M/K114E/K115E}$ and $GP^{L529A/I544A}$ (both also lacking the mucin-like domain), were prepared as previously reported (7, 24, 47).

For some experiments, cleaved viral particles bearing GP_{CL} were first generated by incubation with thermolysin (THL, 1 mg/ml, pH 7.5, 37°C for 1h; Sigma) or recombinant human cathepsin L (CatL, 2 ng/ul, pH 5.5, 37°C for 1h; R&D Systems) as described previously (5). Reactions were stopped by removal onto ice and addition of phosphoramidon (1 mM; Peptides International) or E-64 (10 µm; Peptides International), respectively. While viral particles cleaved with CatL were used immediately, THL-cleaved virus was kept at -80°C until usage.

Antibodies. For immunofluorescence analysis, NPC1-eBFP2 was detected by a rabbit anti-BFP antibody (GeneTex) followed by a secondary anti-rabbit antibody-Alexa 405 or -Alexa 488 fluorophore (Thermo Scientific). During proximity ligation assay (PLA), NPC1 was detected by mAb-548, whose generation was described earlier (17). Detection of proteolytically cleaved GP was carried out with a RBS-specific human anti GP antibody, MR72, either followed by a secondary anti-human antibody-Alexa 555 fluorophore or following the PLA protocol as described below. To detect EBOV GP by immunofluorescence analysis and to determine the effect of GP-targeting antibodies on GP_{CL}:NPC1 interaction we used the previously described human anti-GP antibodies KZ52, mAb100, ADI-15946, and ADI-16061 (28–32). For production of KZ52, ADI-15946, and ADI-16061, variable heavy- and light-chain domain sequences were cloned into the

403 mammalian expression vectors pMAZ-IgL (encoding for the expression cassette of
404 human κ light-chain constant domains) and pMAZ-IgH (encoding for the expression
405 cassette of human γ1 chain constant domains). Antibody production in FreeStyle™ 293-
406 F cells (ThermoFisher) and subsequent purification were carried out as described earlier
407 (17).
408
409 **Inhibitors.** Stock solutions of drugs were prepared in dimethyl sulfoxide (DMSO) and
410 stored as frozen aliquots until use. Cells were incubated with 3.47 (Microbiotix),
411 Amiodarone (Sigma), Bepridil (Sigma), Clomifene (Sigma), Sertraline (Toronto Research
412 Chemicals), or Toremifene (Sigma) for 1 h or 16 h at 37°C with concentrations as
413 indicated. Incubation of cells with E-64d (Peptides International) was extended to 6 h at
414 37°C, while cells were not preincubated with U18666A (Calbiochem) for PLA, but
415 preincubated for 1 h or 16 h at 37°C for additional described experiments at
416 concentrations indicated. Inhibitors were maintained at the same concentrations during
417 virus spin-oculation and virus entry into cells.
418
419 **Generation of U2OS *CatB/L* double knockout cells overexpressing NPC1.** U2OS
420 cells were transduced with a lentivirus carrying human codon-optimized *Streptomyces*
421 *pyogenes* Cas9 (spCas9) and blasticidin resistance genes to generate U2OS-Cas9 cells
422 expressing Cas9. Briefly, 293FT cells were co-transfected with Cas9-expressing plasmid
423 lentiCas9-Blast (Addgene #52962, a gift from Feng Zhang), the lentiviral packaging
424 plasmid psPAX2 (Addgene #12260, a gift from Didier Trono) and a VSV G expressing
425 plasmid. The supernatant filtered through a 0.45 μm filter was used to transduce U2OS

cells in the presence of 6 µg/ml of polybrene and transduced cells were selected with 15 µg/ml of blasticidin. A lentiGuide-Puro plasmid (Addgene plasmid #52963, a gift from Feng Zhang) expressing human *CatL*-targeting sgRNA (5'-CTTAGGGATGTCCACAAAGC-3', targets anti-sense strand, nt 1021-1040 of the *CatL* transcript variant 1 mRNA or nt 4205-4186 of *CatL* gene ID 1514) was used to generate lentiviruses as described above. U2OS-Cas9 cells transduced with these lentiviruses were selected with 2 µg/ml of puromycin. Editing of the *CatL* gene was confirmed by Sanger sequencing of a 673-bp amplicon using primers flanking the sgRNA target site. A single cell clone carrying a homozygous deletion of 15 nucleotides that is predicted to disrupt a critical N-glycosylation site (204-NDT-206) that is required for lysosomal targeting of CatL by causing a T206I change (along with a deletion of aa 207-210) was selected (48, 49). Absence of wild-type allele from the *CatL* knockout (KO) cells was confirmed by RT-PCR using primers specific for the 15-nt deletion. To generate the *CatB/L* double KO, the *CatL*-KO cells were further transduced with a lentivirus encoding *CatB*-specific sgRNA (5'-TTGACCAGCTCATCCGACAG-3', targets anti-sense strand, nt 251-270 of human *CatB* transcript variant 1 mRNA or nt 14,791-14,772 of human *CatB* gene ID 1508). A single cell clone carrying an insertion of a single nucleotide (T) that is predicted to cause a frame-shift leading to a truncated pro-peptide of 28 amino acids (frame shift at aa position 27) was selected. Absence of *CatB* and *CatL* activity in this single cell clone was confirmed by cathepsin activity assays (described below). Stable U2OS cells expressing NPC1 C-terminally tagged with a triple flag sequence in the *CatB/L*-KO background were generated as described earlier. In short, retroviruses packaging the transgene were produced by triple transfection of 293T cells, and target

U2OS cells were directly exposed to sterile-filtered retrovirus-laden supernatants in the presence of polybrene (6 µg/ml). Transduced cell populations were selected with puromycin (2 µg/ml) and expression of flag-tagged NPC1 was confirmed by immunostaining with an anti-Flag M2 antibody (Sigma).

Cathepsin L and B activity assay. U2OS-Cas9, U2OS *CatL*-KO, U2OS *CatB*-KO, and U2OS *CatB*/*L*-KO cells stably expressing flag-tagged NPC1 were lysed (50 mM MES [pH 5.5], 135 mM NaCl, 2 mM ethylenediaminetetraacetic acid [EDTA], 0.5% Triton X-100) for 1 h on ice. As a control, cleared U2OS-Cas9 lysates were pre-incubated with the protease inhibitor E-64 (20 µM; Peptides International) for 20 min at room temperature (when indicated). Then, lysates were mixed with reaction buffer (100 mM NaAcetate [pH 5], 1 mM EDTA, 4 mM dithiothreitol), incubated with the fluorogenic peptide substrate Z-FR-AMC (150 µM; R&D Systems) and measured at a fluorometer following a 0 to 30 min incubation (λ_{Ex} = 390 nm, λ_{Em} = 460 nm). Measurements of substrate hydrolysis were normalized to maximum hydrolysis on U2OS-Cas9 cells reached after 30 min; data represents the mean value and standard deviations of three independent experiments (*n* = 3).

Infection experiments. Confluent U2OS cells were infected with pre-titrated amounts of pseudotyped VSV particles bearing wild-type or mutant GPs. Prior to infection, VSVs were diluted in corresponding media, and infected cells were maintained at 37°C for 14 to 16 h post infection before manual counting of $eGFP^+$ and mNG^+ cells or automated counting using a Cytation 5 cell imaging multi-mode reader (BioTek Instruments) and a

CellInsight CX5 imager (Thermo Fisher) including onboard software. When indicated, cells were pre-incubated with small molecule inhibitors diluted in corresponding media; for antibody neutralization experiments, VSV particles were incubated with increasing concentrations of test Ab at room temperature for 1 h, prior to addition to cell monolayers. Virus infectivities were measured as described above. Virus neutralization data was subjected to nonlinear regression analysis (4-parameter, variable slope sigmoidal dose-response equation; GraphPad Prism).

Immunofluorescence microscopy and immunostaining. To investigate determinants of VSV mNG-P EBOV GP internalization into endosomal compartments, pre-titrated amounts of VSV particles bearing mNG-P and either wild-type or mutant EBOV GP were diluted into imaging buffer (20 mM HEPES [pH 7.4], 140 mM NaCl, 2.5 mM KCl, 1.8 mM $CaCl_2$, 1 mM $MgCl_2$, 5 mM glucose, 2% FBS), and spin-occulated onto pre-chilled $U2OS^{NPC1\text{-}eBFP2}$ cells on coverslips. Unbound virus was removed by washing with cold PBS. Cells were then placed in warm imaging buffer, and allowed to internalize VSVs for 1 h at 37°C. Cells were fixed with 3.7% paraformaldehyde and permeabilized with PBS/0.1% Triton X-100. NPC1-eBFP2 was detected with either primary mouse anti-NPC1 mAb-548 or rabbit anti-BFP antibodies and secondary anti-mouse or anti-rabbit antibody-Alexa 405 fluorophore conjugates, respectively (Thermo Scientific). Cleaved GP was detected with the primary mouse RBS-specific anti-GP antibody MR72 followed by secondary anti-mouse antibody-Alexa 555 fluorophore conjugate (Thermo Scientific). To investigate transport of IgGs bound to VSV particles into $NPC1^+$ endosomal compartments, VSV particles bearing mNG-P were preincubated with antibodies (50 or

100 µg/ml, respectively) for 1 h at room temperature, followed by internalization into target cells and detection by incubation with secondary anti-human-Alexa 555 fluorophore conjugates (Thermo Scientific). Cells were examined by immunofluorescence analysis performed on an Axio Observer Z1 widefield epifluorescence microscope (Zeiss Inc.) equipped with an ORCA- Flash4.0 LT digital CMOS camera (Hamamatsu Photonics), a 63x/1.4 numerical aperture oil immersion objective and a DAPI (4′,6-diamidino-2-phenylindole)/fluorescein isothiocyanate (FITC)/tetramethyl rhodamine isocyanate (TRITC)/Cy5 filter set. Images were processed in Photoshop (Adobe Systems).

Cholesterol accumulation assay. Cholesterol accumulation following inhibitor treatment of U2OS$^{NPC1\text{-}eBFP2}$ cells was monitored by incubation with filipin (50 µg/ml; Sigma) for 1 h at room temperature. Cells were examined by immunofluorescence analysis as described under the method section 'Immunofluorescence microscopy and immunostaining'.

Proximity Ligation Assay. U2OS$^{NPC1\text{-}eBFP2}$ cells were allowed to internalize VSV particles (in the presence or absence of small molecule inhibitors or antibodies), fixed and permeabilized as described in the method section 'Immunofluorescence microscopy and immunostaining'. MR72, a RBS-targeting anti-GP mAb and mAb-548, an NPC1 domain C-targeting mAb were directly labeled with Duolink® In Situ Probemaker PLUS and Duolink® In Situ Probemaker MINUS (Sigma) following the manufacturer's instructions. Fixed cells were incubated with labeled antibodies in a humidity chamber

518 at 37°C for 1 h. Excess antibody was removed by washing with Duolink® In Situ Wash
519 Buffer (Sigma). GP:NPC1 interaction was detected by applying the Duolink® In Situ
520 Detection Reagents Red kit following the manufacturer's instructions (Sigma). After
521 removing excess reagents, NPC1-eBFP2 was detected using a rabbit anti-BFP antibody
522 followed by a secondary anti-rabbit antibody-Alexa 405 fluorophore conjugate (Thermo
523 Fisher). Cells were examined by immunofluorescence analysis as described under the
524 method section 'Immunofluorescence microscopy and immunostaining'.
525
526 **ACKNOWLEDGMENTS**
527
528 We acknowledge Isabel Gutierrez, Estefania Valencia, Laura Polanco, and Cecelia
529 Harold for laboratory management and technical support. This work was supported by
530 National Institutes of Health (NIH) grant R01AI134824 (to K.C.). K.C. is a member of the
531 Scientific Advisory Board of Integrum Scientific, LLC.
532
533 **REFERENCES**
534
535 1. Feldmann H, Geisbert TW. 2011. Ebola haemorrhagic fever. Lancet
536 377:849–862.
537 2. WHO. 2020. Ebola Virus Disease - Democratic Republic of the Congo.
538 External Situation Report 88.
539 3. Saeed MF, Kolokoltsov AA, Albrecht T, Davey RA. 2010. Cellular entry of
540 ebola virus involves uptake by a macropinocytosis-like mechanism and subsequent

541 trafficking through early and late endosomes. PLoS Pathog 6:e1001110.

542 4. Mulherkar N, Raaben M, de la Torre JC, Whelan SP, Chandran K. 2011.
543 The Ebola virus glycoprotein mediates entry via a non-classical dynamin-dependent
544 macropinocytic pathway. Virology 419:72–83.

545 5. Spence JS, Krause TB, Mittler E, Jangra RK, Chandran K. 2016. Direct
546 visualization of ebola virus fusion triggering in the endocytic pathway. MBio
547 7:e01857-15.

548 6. Nanbo A, Imai M, Watanabe S, Noda T, Takahashi K, Neumann G,
549 Halfmann P, Kawaoka Y. 2010. Ebolavirus is internalized into host cells via
550 macropinocytosis in a viral glycoprotein-dependent manner. PLoS Pathog
551 6:e1001121.

552 7. Chandran K, Sullivan NJ, Felbor U, Whelan SP, Cunningham JM. 2005.
553 Endosomal proteolysis of the Ebola virus glycoprotein is necessary for infection.
554 Science 308:1643–1645.

555 8. Schornberg K, Matsuyama S, Kabsch K, Delos S, Bouton A, White J. 2006.
556 Role of endosomal cathepsins in entry mediated by the Ebola virus glycoprotein. J
557 Virol 80:4174–4178.

558 9. Misasi J, Chandran K, Yang J-Y, Considine B, Filone CM, Côté M, Sullivan
559 N, Fabozzi G, Hensley L, Cunningham J. 2012. Filoviruses require endosomal
560 cysteine proteases for entry but exhibit distinct protease preferences. J Virol
561 86:3284–3292.

562 10. Carette JE, Raaben M, Wong AC, Herbert AS, Obernosterer G, Mulherkar
563 N, Kuehne AI, Kranzusch PJ, Griffin AM, Ruthel G, Dal Cin P, Dye JM, Whelan SP,

564 Chandran K, Brummelkamp TR. 2011. Ebola virus entry requires the cholesterol
565 transporter Niemann-Pick C1. Nature 477:340–343.
566 11. Miller EH, Obernosterer G, Raaben M, Herbert AS, Deffieu MS, Krishnan
567 A, Ndungo E, Sandesara RG, Carette JE, Kuehne AI, Ruthel G, Pfeffer SR, Dye
568 JM, Whelan SP, Brummelkamp TR, Chandran K. 2012. Ebola virus entry requires
569 the host-programmed recognition of an intracellular receptor. EMBO J 31:1947–
570 1960.
571 12. Côté M, Misasi J, Ren T, Bruchez A, Lee K, Filone CM, Hensley L, Li Q,
572 Ory D, Chandran K, Cunningham J. 2011. Small molecule inhibitors reveal
573 Niemann-Pick C1 is essential for Ebola virus infection. Nature 477:344–348.
574 13. Ng M, Ndungo E, Jangra RK, Cai Y, Postnikova E, Radoshitzky SR, Dye
575 JM, Ramírez de Arellano E, Negredo A, Palacios G, Kuhn JH, Chandran K. 2014.
576 Cell entry by a novel European filovirus requires host endosomal cysteine proteases
577 and Niemann-Pick C1. Virology 468–470:637–646.
578 14. Goldstein T, Anthony SJ, Gbakima A, Bird BH, Bangura J, Tremeau-
579 Bravard A, Belaganahalli MN, Wells HL, Dhanota JK, Liang E, Grodus M, Jangra
580 RK, DeJesus VA, Lasso G, Smith BR, Jambai A, Kamara BO, Kamara S, Bangura
581 W, Monagin C, Mazet JAK. 2018. The discovery of Bombali virus adds further
582 support for bats as hosts of ebolaviruses. Nat Microbiol 3:1084–1089.
583 15. Bale S, Liu T, Li S, Wang Y, Abelson D, Fusco M, Woods VL, Saphire EO.
584 2011. Ebola virus glycoprotein needs an additional trigger, beyond proteolytic
585 priming for membrane fusion. PLoS Negl Trop Dis 5:e1395.
586 16. Shoemaker CJ, Schornberg KL, Delos SE, Scully C, Pajouhesh H, Olinger

587 GG, Johansen LM, White JM. 2013. Multiple cationic amphiphiles induce a
588 Niemann-Pick C phenotype and inhibit Ebola virus entry and infection. PLoS ONE
589 8:e56265.
590 17. Wec AZ, Nyakatura EK, Herbert AS, Howell KA, Holtsberg FW, Bakken RR,
591 Mittler E, Christin JR, Shulenin S, Jangra RK, Bharrhan S, Kuehne AI, Bornholdt
592 ZA, Flyak AI, Saphire EO, Crowe JE, Aman MJ, Dye JM, Lai JR, Chandran K. 2016.
593 A “Trojan horse” bispecific-antibody strategy for broad protection against
594 ebolaviruses. Science 354:350–354.
595 18. Bornholdt ZA, Ndungo E, Fusco ML, Bale S, Flyak AI, Crowe JE, Chandran
596 K, Saphire EO. 2015. Host-Primed Ebola Virus GP Exposes a Hydrophobic NPC1
597 Receptor-Binding Pocket, Revealing a Target for Broadly Neutralizing Antibodies.
598 MBio 7.
599 19. Flyak AI, Ilinykh PA, Murin CD, Garron T, Shen X, Fusco ML, Hashiguchi T,
600 Bornholdt ZA, Slaughter JC, Sapparapu G, Klages C, Ksiazek TG, Ward AB,
601 Saphire EO, Bukreyev A, Crowe JE. 2015. Mechanism of human antibody-mediated
602 neutralization of Marburg virus. Cell 160:893–903.
603 20. Fredriksson S, Gullberg M, Jarvius J, Olsson C, Pietras K, Gústafsdóttir SM,
604 Ostman A, Landegren U. 2002. Protein detection using proximity-dependent DNA
605 ligation assays. Nat Biotechnol 20:473–477.
606 21. Gullberg M, Fredriksson S, Taussig M, Jarvius J, Gustafsdottir S,
607 Landegren U. 2003. A sense of closeness: protein detection by proximity ligation.
608 Curr Opin Biotechnol 14:82–86.
609 22. Wang H, Shi Y, Song J, Qi J, Lu G, Yan J, Gao GF. 2016. Ebola Viral

610 Glycoprotein Bound to Its Endosomal Receptor Niemann-Pick C1. Cell 164:258–
611 268.
612 23. Fels JM, Spence JS, Bortz RH, Bornholdt ZA, Chandran K. 2019. A
613 hyperstabilizing mutation in the base of the ebola virus glycoprotein acts at multiple
614 steps to abrogate viral entry. MBio 10.
615 24. Wong AC, Sandesara RG, Mulherkar N, Whelan SP, Chandran K. 2010. A
616 forward genetic strategy reveals destabilizing mutations in the Ebolavirus
617 glycoprotein that alter its protease dependence during cell entry. J Virol 84:163–
618 175.
619 25. Kaletsky RL, Simmons G, Bates P. 2007. Proteolysis of the Ebola virus
620 glycoproteins enhances virus binding and infectivity. J Virol 81:13378–13384.
621 26. Brecher M, Schornberg KL, Delos SE, Fusco ML, Saphire EO, White JM.
622 2012. Cathepsin cleavage potentiates the Ebola virus glycoprotein to undergo a
623 subsequent fusion-relevant conformational change. J Virol 86:364–372.
624 27. Gregory SM, Harada E, Liang B, Delos SE, White JM, Tamm LK. 2011.
625 Structure and function of the complete internal fusion loop from Ebolavirus
626 glycoprotein 2. Proc Natl Acad Sci USA 108:11211–11216.
627 28. Misasi J, Gilman MSA, Kanekiyo M, Gui M, Cagigi A, Mulangu S, Corti D,
628 Ledgerwood JE, Lanzavecchia A, Cunningham J, Muyembe-Tamfun JJ, Baxa U,
629 Graham BS, Xiang Y, Sullivan NJ, McLellan JS. 2016. Structural and molecular
630 basis for Ebola virus neutralization by protective human antibodies. Science
631 351:1343–1346.
632 29. West BR, Wec AZ, Moyer CL, Fusco ML, Ilinykh PA, Huang K, Wirchnianski

633 AS, James RM, Herbert AS, Hui S, Goodwin E, Howell KA, Kailasan S, Aman MJ,
634 Walker LM, Dye JM, Bukreyev A, Chandran K, Saphire EO. 2019. Structural basis
635 of broad ebolavirus neutralization by a human survivor antibody. Nat Struct Mol Biol
636 26:204–212.
637 30. Wec AZ, Herbert AS, Murin CD, Nyakatura EK, Abelson DM, Fels JM, He
638 S, James RM, de La Vega M-A, Zhu W, Bakken RR, Goodwin E, Turner HL, Jangra
639 RK, Zeitlin L, Qiu X, Lai JR, Walker LM, Ward AB, Dye JM, Bornholdt ZA. 2017.
640 Antibodies from a Human Survivor Define Sites of Vulnerability for Broad Protection
641 against Ebolaviruses. Cell 169:878-890.e15.
642 31. Bornholdt ZA, Turner HL, Murin CD, Li W, Sok D, Souders CA, Piper AE,
643 Goff A, Shamblin JD, Wollen SE, Sprague TR, Fusco ML, Pommert KBJ, Cavacini
644 LA, Smith HL, Klempner M, Reimann KA, Krauland E, Gerngross TU, Wittrup KD,
645 Walker LM. 2016. Isolation of potent neutralizing antibodies from a survivor of the
646 2014 Ebola virus outbreak. Science 351:1078–1083.
647 32. Lee JE, Fusco ML, Hessell AJ, Oswald WB, Burton DR, Saphire EO. 2008.
648 Structure of the Ebola virus glycoprotein bound to an antibody from a human
649 survivor. Nature 454:177–182.
650 33. Gehring G, Rohrmann K, Atenchong N, Mittler E, Becker S, Dahlmann F,
651 Pöhlmann S, Vondran FWR, David S, Manns MP, Ciesek S, von Hahn T. 2014. The
652 clinically approved drugs amiodarone, dronedarone and verapamil inhibit filovirus
653 cell entry. J Antimicrob Chemother 69:2123–2131.
654 34. Johansen LM, DeWald LE, Shoemaker CJ, Hoffstrom BG, Lear-Rooney
655 CM, Stossel A, Nelson E, Delos SE, Simmons JA, Grenier JM, Pierce LT, Pajouhesh

656 H, Lehár J, Hensley LE, Glass PJ, White JM, Olinger GG. 2015. A screen of
657 approved drugs and molecular probes identifies therapeutics with anti-Ebola virus
658 activity. Sci Transl Med 7:290ra89.
659 35. Ren J, Zhao Y, Fry EE, Stuart DI. 2018. Target Identification and Mode of
660 Action of Four Chemically Divergent Drugs against Ebolavirus Infection. J Med
661 Chem 61:724–733.
662 36. DeWald LE, Dyall J, Sword JM, Torzewski L, Zhou H, Postnikova E, Kollins
663 E, Alexander I, Gross R, Cong Y, Gerhardt DM, Johnson RF, Olinger GG, Holbrook
664 MR, Hensley LE, Jahrling PB. 2018. The calcium channel blocker bepridil
665 demonstrates efficacy in the murine model of marburg virus disease. J Infect Dis
666 218:S588–S591.
667 37. Johansen LM, Brannan JM, Delos SE, Shoemaker CJ, Stossel A, Lear C,
668 Hoffstrom BG, Dewald LE, Schornberg KL, Scully C, Lehár J, Hensley LE, White
669 JM, Olinger GG. 2013. FDA-approved selective estrogen receptor modulators inhibit
670 Ebola virus infection. Sci Transl Med 5:190ra79.
671 38. Zhao Y, Ren J, Harlos K, Jones DM, Zeltina A, Bowden TA, Padilla-Parra
672 S, Fry EE, Stuart DI. 2016. Toremifene interacts with and destabilizes the Ebola
673 virus glycoprotein. Nature 535:169–172.
674 39. Lu F, Liang Q, Abi-Mosleh L, Das A, De Brabander JK, Goldstein JL, Brown
675 MS. 2015. Identification of NPC1 as the target of U18666A, an inhibitor of lysosomal
676 cholesterol export and Ebola infection. elife 4.
677 40. Cheshenko N, Pierce C, Herold BC. 2018. Herpes simplex viruses activate
678 phospholipid scramblase to redistribute phosphatidylserines and Akt to the outer

679 leaflet of the plasma membrane and promote viral entry. PLoS Pathog
680 14:e1006766.
681 41. Jambunathan N, Charles A-S, Subramanian R, Saied AA, Naderi M, Rider
682 P, Brylinski M, Chouljenko VN, Kousoulas KG. 2015. Deletion of a Predicted β-
683 Sheet Domain within the Amino Terminus of Herpes Simplex Virus Glycoprotein K
684 Conserved among Alphaherpesviruses Prevents Virus Entry into Neuronal Axons.
685 J Virol 90:2230–2239.
686 42. Zhang P, Monteiro da Silva G, Deatherage C, Burd C, DiMaio D. 2018. Cell-
687 Penetrating Peptide Mediates Intracellular Membrane Passage of Human
688 Papillomavirus L2 Protein to Trigger Retrograde Trafficking. Cell 174:1465-
689 1476.e13.
690 43. Assetta B, Morris-Love J, Gee GV, Atkinson AL, O'Hara BA, Maginnis MS,
691 Haley SA, Atwood WJ. 2019. Genetic and Functional Dissection of the Role of
692 Individual 5-HT2 Receptors as Entry Receptors for JC Polyomavirus. Cell Rep
693 27:1960-1966.e6.
694 44. Takada A, Robison C, Goto H, Sanchez A, Murti KG, Whitt MA, Kawaoka
695 Y. 1997. A system for functional analysis of Ebola virus glycoprotein. Proc Natl Acad
696 Sci USA 94:14764–14769.
697 45. Whelan SP, Ball LA, Barr JN, Wertz GT. 1995. Efficient recovery of
698 infectious vesicular stomatitis virus entirely from cDNA clones. Proc Natl Acad Sci
699 USA 92:8388–8392.
700 46. Jeffers SA, Sanders DA, Sanchez A. 2002. Covalent modifications of the
701 ebola virus glycoprotein. J Virol 76:12463–12472.

47. Kleinfelter LM, Jangra RK, Jae LT, Herbert AS, Mittler E, Stiles KM, Wirchnianski AS, Kielian M, Brummelkamp TR, Dye JM, Chandran K. 2015. Haploid genetic screen reveals a profound and direct dependence on cholesterol for hantavirus membrane fusion. MBio 6:e00801.

48. Smith SM, Kane SE, Gal S, Mason RW, Gottesman MM. 1989. Glycosylation of procathepsin L does not account for species molecular-mass differences and is not required for proteolytic activity. Biochem J 262:931–938.

49. Kane SE. 1993. Mouse procathepsin L lacking a functional glycosylation site is properly folded, stable, and secreted by NIH 3T3 cells. J Biol Chem 268:11456–11462.

FIGURE LEGENDS

Fig. 1. Development of an EBOV GP:NPC1 binding assay in intact cells by *in situ* proximity ligation. (**A**) VSV mNG-P particles bearing EBOV GP were internalized into U2OS cells ectopically expressing NPC1-eBFP2 for 60 min. Cells were fixed, permeabilized and subjected to proximity ligation assay (PLA) using GP_{CL}- and NPC1-specific antibodies (MR72/mAb-548). During amplification, resulting PLA products were labeled with a detector oligonucleotide conjugated with a red fluorophore. White arrowheads, VSV/NPC1 colocalization; red arrowheads, VSV/NPC1/PLA colocalization. (**B**) VSVs bearing EBOV GP were endocytosed into U2OS cells as described in (A), fixed at the indicated time points and subjected to PLA. VSV positive compartments (VSV^+) were enumerated; the percentage of compartments also positive for NPC1 ($VSV^+/NPC1^+$)

or NPC1 plus PLA ($VSV^+/NPC1^+/PLA^+$) were determined. Representative curves out of two independent experiments are shown; averages of pooled cells are displayed ($n \geq 20$ per time point).

Fig. 2. Proximity ligation is sensitive to perturbations in the GP_{CL}:NPC1 domain C interface. (**A**) VSV mNG-P particles bearing EBOV GP or EBOV $GP^{T83M/K114E/K115E}$ were internalized into $U2OS^{NPC1\text{-}eBFP2}$ cells for 60 min followed by cell fixation, permeabilization and PLA. Cells were analyzed by fluorescence microscopy; data points represent the percentage of $VSV^+/NPC1^+/PLA^+$ compartments per individual cell; bars depict the pooled averages and standard deviations (± SD) for all cells from two independent experiments ($n \geq 40$). An unpaired two-tailed t-test was used to compare $VSV^+/NPC1^+/PLA^+$ compartments of cells infected by VSV bearing either EBOV GP or EBOV $GP^{T83M/K114E/K115E}$ (****, $P < 0.0001$). Group means calculated from the percentage of $VSV^+/NPC1^+/PLA^+$ vesicles were compared by Cohen's *d* effect size ($d > 1.3$). (**B**) $U2OS^{NPC1\text{-}eBFP2}$ cells were pre-incubated with the inhibitor 3.47 (1 µM) for 60 min at 37°C, followed by VSV mNG-P EBOV GP uptake for 60 min and PLA. Data points were acquired and analyzed as described in (A). (**C**) After pre-incubation of $U2OS^{NPC1\text{-}eBFP2}$ and wild-type U2OS cells with increasing 3.47 concentrations, cells were infected with VSV mNG-P EBOV GP for 16 h. Infection was measured by automated counting of mNG^+ cells and normalized to infection obtained in the absence of 3.47. Averages ± SD for six technical replicates pooled from two independent experiments are displayed. Data was

746 subjected to nonlinear regression analysis to derive 3.47 concentration at half-maximal
747 inhibition of infection (IC_{50} ± 95% confidence intervals for nonlinear curve fit).
748
749 **Fig. 3.** Detection of GP_{CL}:NPC1 binding by PLA requires endosomal cleavage of GP. (**A**)
750 VSV mNG-P particles bearing EBOV GP were incubated with either $U2OS^{NPC1\text{-}eBFP2}$ cells
751 pre-treated with E-64d (100mM, 6h at 37°C) (left panel), or U2OS *CatB/L*-KO cells
752 ectopically over- expressing flag-tagged NPC1 (right panel). Cells were fixed following
753 virus incubation (1 h at 37°C), permeabilized and subjected to PLA. Data points represent
754 the percentage of $VSV^+/NPC1^+/PLA^+$ compartments per individual cell; bars depict the
755 average ±SD for all data points pooled from two independent experiments ($n \geq 30$).
756 Points with reduced transparency represent values outside of the 10th-90th percentile.
757 An unpaired two-tailed t-test was used to compare $VSV^+/NPC1^+/PLA^+$ compartments of
758 wild-type cells with either inhibitor- treated (left) or KO (right) cells infected by EBOV GP-
759 decorated VSV (****, $P < 0.0001$). Group means calculated from the percentage of
760 $VSV^+/NPC1^+/PLA^+$ vesicles were compared by Cohen's *d* effect size. (**B**) Cells described
761 in (A) were exposed to VSV mNG-P EBOV GP uptake for 1h at 37°C. After fixation, viral
762 particles, NPC1 and GP_{CL} were visualized by fluorescence microscopy. Representative
763 images from two independent experiments are shown. (**C**) VSV mNG-P particles bearing
764 EBOV GP were treated *in vitro* with thermolysin (THL) or cathepsin L (CatL), respectively.
765 Viral particles were taken up into $U2OS^{NPC1\text{-}eBFP2}$ cells, followed by fixing of the cells and
766 subjecting them to PLA. Data points represent the percentage of $VSV^+/NPC1^+/PLA^+$
767 compartments per individual cell; bars depict the average ±SD for all data points pooled
768 from two independent experiments ($n \geq 25$). To compare $VSV^+/NPC1^+/PLA^+$

769 compartments of cells which endocytosed VSV studded with either uncleaved or
770 THL/CatL- cleaved GP, an unpaired two-tailed *t*-test was used (****, $P < 0.0001$). Cohen's
771 *d* effect size was used to compare the group means calculated from the percentages of
772 $VSV^+/NPC1^+/PLA^+$ vesicles ($d > 1.3$). (**D**) $U2OS^{NPC1\text{-}eBFP2}$ cells were (not) pre-incubated with
773 E-64d (as described in [A]) and VSV mNG-P particles bearing EBOV GP were treated *in*
774 *vitro* with THL. Following virus internalization into $U2OS^{NPC1\text{-}eBFP2}$, cells were fixed and
775 subjected to PLA. Data points represent the percentage of $VSV^+/NPC1^+/PLA^+$
776 compartments per individual cell; bars depict the average ±SD for all data points pooled
777 from two independent experiments ($n \geq 25$). Points with reduced transparency represent
778 values outside of the 10th-90th percentile. To compare $VSV^+/NPC1^+/PLA^+$ compartments
779 of E-64d-treated cells with those of untreated cells which endocytosed VSV studded
780 with either uncleaved or THL-cleaved GP, an unpaired two-tailed *t*-test was used (**, P
781 < 0.01; ***, $P < 0.001$; ****, $P < 0.0001$). Cohen's *d* effect size was used to compare the
782 group means calculated from the percentages of $VSV^+/NPC1^+/PLA^+$ vesicles.
783
784 **Fig. 4.** *In situ* proximity ligation decouples GP_{CL}:NPC1 interaction from post-binding
785 entry steps. (**A**) VSV mNG-P particles bearing EBOV GP or EBOV $GP^{L529A/I544A}$ were
786 internalized into $U2OS^{NPC1\text{-}eBFP2}$ cells for 60 min followed by PLA. Data points represent
787 the percentage of triple positive compartments per individual cell; bars depict the
788 average ±SD for all data points pooled from two independent experiments ($n \geq 37$). Data
789 analyses included an unpaired two-tailed t-test to compare $VSV^+/NPC1^+/PLA^+$ vesicles
790 of cells which internalized VSV decorated with wild-type or mutant GP (ns, $P > 0.05$).

Cohen's *d* effect size was used to compare the group means calculated from the percentages of $VSV^+/NPC1^+/PLA^+$ compartments. (**B**) ADI-15946 was incubated with VSV EBOV GP particles and exposed to $U2OS^{NPC1\text{-}eBFP2}$ (right panel). After virus uptake for 1 h at 37°C, cells were fixed and viral particles, NPC1 and bound antibodies were visualized by fluorescence microscopy. Representative images from two independent experiments are shown. Virions were preincubated with increasing amounts of KZ52, mAb100, ADI-15946 or ADI-16061 and then exposed to $U2OS^{NPC1\text{-}eBFP2}$ cells for 16 h at 37°C (left panel). Number of infected cells was determined by automated counting of mNG^+ cells and normalized to infection obtained in the absence of antibodies. Averages ± SD for six technical replicates pooled from two independent experiments are shown. (**C**) VSV mNG-P EBOV GP virions were complexed with KZ52, mAb100, ADI-15946 or ADI-16061 (50 µg/ml and 100 µg/ml) for 1 h at room temperature. Following internalization into $U2OS^{NPC1\text{-}eBFP2}$, cells were fixed, and subjected to *in situ* PLA. Data points represent the percentage of $VSV^+/NPC1^+/PLA^+$ compartments per individual cell; bars show the average ±SD for all data points pooled from two independent experiments ($n \geq 22$). $VSV^+/NPC1^+/PLA^+$ vesicles were analyzed by unpaired two-tailed t-test (ns, $P > 0.05$; *, $P < 0.05$; **, $P < 0.01$; ****, $P < 0.0001$) comparing cells which were exposed to virion-antibody complexes to cells exposed to untreated virus. Group means calculated from the percentage of $VSV^+/NPC1^+/PLA^+$ vesicles were also compared by Cohen's *d* effect size.

Fig. 5. Small molecule inhibitor-mediated selective interference of GP:NPC1 binding delineated by *in situ* PLA. (**A**) $U2OS^{NPC1\text{-}eBFP2}$ cells were preincubated with increasing

814 concentrations of amiodarone, bepridil, clomifene, sertraline, toremifene, and U18666A,
815 respectively before exposed to VSV mNG-P EBOV GP for 16 h at 37°C. Infection was
816 measured by automated counting of mNG^+ cells and normalized to infection obtained in
817 the presence of vehicle only. Averages ± SD for nine to eighteen technical replicates
818 pooled from three to six independent experiments are displayed. (**B**) $U2OS^{NPC1\text{-}eBFP2}$ cells
819 were incubated with amiodarone, bepridil, clomifene, and sertraline, respectively (2 μM
820 or 5 μM, 1 h at 37°C), or toremifene (2 μM or 10 μM, 1 h at 37°C), or U18666A (10 μM, 2
821 h at 37°C), followed by VSV mNG-P EBOV GP uptake for 1 h. Cells were subjected to *in*
822 *situ* PLA and analyzed by fluorescence microscopy. The percentage of triple positive
823 $VSV^+/NPC1^+/PLA^+$ compartments per individual cell is represented by data points; bars
824 show the average ±SD for all data points pooled from two independent experiments (n
825 $\geq$ 20). $VSV^+/NPC1^+/PLA^+$ vesicles were analyzed by unpaired two-tailed t-test (ns, $P >$
826 0.05; *, $P < 0.05$; ****, $P < 0.0001$) comparing inhibitor-exposed to untreated cells. Group
827 means calculated from the percentage of $VSV^+/NPC1^+/PLA^+$ compartments were also
828 compared by Cohen's d effect size. (**C**) Table summarizing results from Fig. 5B and Fig.
829 S6.
830
831 **Fig. S1.** PLA requires the presence of both detecting antibodies and VSV internalization.
832 VSV mNG-P particles bearing EBOV GP were exposed to $U2OS^{NPC1\text{-}eBFP2}$ cells for 1 h at
833 37°C or, to inhibit endocytosis, at 4°C. Cells were fixed, permeabilized and subjected to
834 *in situ* PLA using GP_{CL}-specific (MR72) or NPC1 domain C-specific (mAb-548) antibodies
835 only, or a combination of both. The percentage of $VSV^+/NPC1^+/PLA^+$ compartments per
836 cell was determined by fluorescence microscopy and presented here by individual data

837 points. Graphic bars show the average ±SD for all data points pooled from one to two
838 independent experiments ($n \geq 10$).
839
840 **Fig. S2.** GP_{CL}:NPC1 interface formation is required for *in situ* PLA. (**A**) VSV particles
841 bearing EBOV GP or EBOV $GP^{T83M/K114E/K115E}$ were exposed to $U2OS^{NPC1\text{-}eBFP2}$ cells for 1 h
842 at 37°C. After fixation, viral particles, NPC1 and GP_{CL} were visualized by fluorescence
843 microscopy. Representative images from two independent experiments are shown. (**B**)
844 Virions bearing EBOV GP or EBOV $GP^{T83M/K114E/K115E}$ normalized for the VSV matrix protein
845 M (data not shown) were used to infect $U2OS^{NPC1\text{-}eBFP2}$ cells. Infection was measured by
846 manual counting of mNG^+ cells and normalized to infection with VSV mNG-P decorated
847 with wild-type GP. Averages ± SD for four technical replicates pooled from two
848 independent experiments are presented. (**C**) After incubation of $U2OS^{NPC1\text{-}eBFP2}$ cells with
849 3.47 (1 μM, 1 h at 37°C), cells were either directly fixed or exposed to VSV mNG-P EBOV
850 GP for 1 h at 37°C prior to fixation. NPC1 was detected by mAb-548 (upper panel) and
851 GP_{CL} was detected by MR72 (lower panel). Representative images of fluorescence
852 microscopy from two independent experiments are shown.
853
854 **Fig. S3.** Endosomal protease activity is essential for EBOV GP-mediated particle
855 infectivity. (**A**) $U2OS^{NPC1\text{-}eBFP2}$ cells were treated with E-64d (100 mM, 6 h at 37°C) followed
856 by infection with VSV bearing EBOV GP. Number of infected cells was determined by
857 manual counting of mNG^+ cells and normalized to infection obtained in the presence of
858 vehicle only. Averages ± SD for four technical replicates pooled from two independent

859 experiments are presented. (**B**) After *in vitro* treatment of VSV mNG-P EBOV GP particles
860 with thermolysin (THL) or cathepsin L (CatL), virions were normalized by a quantitative
861 Western Blot assay detecting VSV M and exposed to U2OS$^{NPC1\text{-}eBFP2}$ cells. Number of
862 infected cells was determined by manual counting of mNG^{+} cells and normalized to
863 infection obtained with untreated VSV mNG-P EBOV GP. Averages ± SD for four
864 technical replicates pooled from two independent experiments are presented.
865
866 **Fig. S4.** Characterization of CRISPR/Cas9-generated U2OS *CatB/L*-KO cells. (**A**)
867 Alignment of the wild-type *Cat L* and *B* gene sequences with alleles in the *CatB/L*-KO
868 cell clone. The gRNA target sequence is depicted in red, the PAM sequence is depicted
869 in blue. (**B**) *CatB* and *CatL* activities in U2OS cell extracts were measured by fluorogenic
870 peptide turnover. As a control, the proteolytic activity in U2OS *CatL*- or *CatB*-KO cells
871 and U2OS cells which were pretreated for 20min with 20 µM E-64d was also determined.
872 Averages ± SD for six technical replicates pooled from two independent experiments are
873 presented. (**C**) Susceptibility of U2OS *CatB/L*-KO cells and U2OS *CatB/L*-KO cells
874 ectopically overexpressing flag-tagged NPC1 to EBOV GP and VSV G-mediated VSV
875 infection. Number of infected cells was determined by manual counting of eGFP^{+} or
876 mNG^{+} cells and normalized to infection obtained with wild-type U2OS cells.
877
878 **Fig. S5.** *In situ* PLA allows decoupling of GP:NPC1 binding from post-NPC1 binding
879 steps. (**A**) VSV mNG-P particles studded with EBOV GP or EBOV GP$^{L529A/I544A}$ were
880 internalized into U2OS$^{NPC1\text{-}eBFP2}$ cells for 1 h. Following fixation, viral particles, NPC1 and

881 GP_{CL} were visualized by fluorescence microscopy. Representative images from two
882 independent experiments are shown. (**B**) Virions bearing EBOV GP were first complexed
883 with KZ52, mAb100 or ADI-16061 antibodies (50µg/ml) for 1 h at room temperature, and
884 then virus-antibody complexes were internalized into $U2OS^{NPC1\text{-}eBFP2}$ cells. By
885 fluorescence microscopy, viral particles, NPC1 and bound antibodies were visualized.
886 (**C**) Samples were generated as described in (B) and viral particles, NPC1 and GP_{CL} (via
887 MR72) were visualized by fluorescence microscopy.
888
889 **Fig. S6.** Small molecule inhibitors interfere with cell susceptibility to infection, virus
890 trafficking as well as NPC1 distribution and function. (**A**) Wild-type U2OS or $U2OS^{NPC1\text{-}}$
891 ^{eBFP2} cells were preincubated with increasing amounts of indicated inhibitors and then
892 exposed to VSV decorated with EBOV GP for 16 h at 37°C in presence of the inhibitors.
893 Number of infected cells was determined by automated counting of $eGFP^+$ cells and
894 normalized to infection obtained in the absence of inhibitors. Averages for six technical
895 replicates pooled from two independent experiments are shown. (**B**) As outlined in Fig.
896 5B, $U2OS^{NPC1\text{-}eBFP2}$ cells were incubated with amiodarone, bepridil, clomifene, toremifene,
897 sertraline, and U18666A respectively, followed by VSV mNG-P EBOV GP uptake for 1 h.
898 Cells were subjected to *in situ* PLA and analyzed by fluorescence microscopy. The
899 percentage of double positive $VSV^+/NPC1^+$ compartments per individual cell is
900 represented by data points; bars show the average ±SD for all data points pooled from
901 two independent experiments ($n \geq 20$). $VSV^+/NPC1^+$ vesicles were analyzed by unpaired
902 two-tailed *t*-test (ns, $P > 0.05$; *, $P < 0.05$; ***, $P < 0.001$; ****, $P < 0.0001$) comparing

inhibitor-exposed to vehicle treated cells. (**C**) U2OS$^{NPC1\text{-}eBFP2}$ cells were incubated with U18666A (10μM), amiodarone (5μM), clomifene (5μM) or DMSO carrier for 16 h at 37°C, followed by detection of NPC1 by mAb-548 (bottom panels) or NPC1 detection followed by filipin staining highlighting cholesterol accumulations (top panels) and analyzed by fluorescence microscopy.

Fig. 1

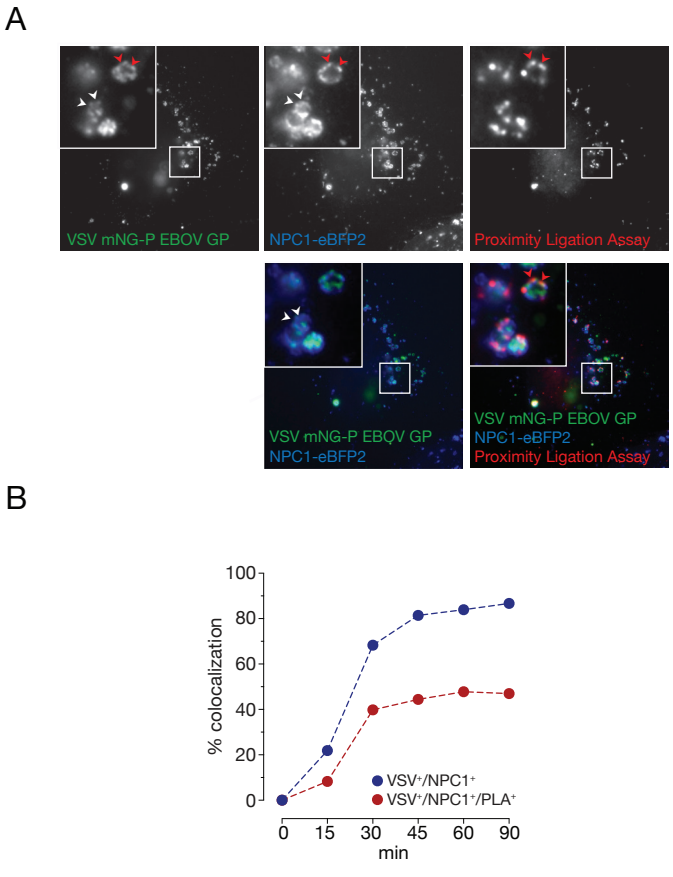

Fig. 1. Development of an EBOV GP:NPC1 binding assay in intact cells by *in situ* proximity ligation. (**A**) VSV mNG-P particles bearing EBOV GP were internalized into U2OS cells ectopically expressing NPC1-eBFP2 for 60 min. Cells were fixed, permeabilized and subjected to proximity ligation assay (PLA) using GP_{CL}- and NPC1-specific antibodies (MR72/mAb-548). During amplification, resulting PLA products were labeled with a detector oligonucleotide conjugated with a red fluorophore. White arrowheads, VSV/NPC1 colocalization; red arrowheads, VSV/NPC1/PLA colocalization. (**B**) VSVs bearing EBOV GP were endocytosed into U2OS cells as described in (A), fixed at the indicated time points and subjected to PLA. VSV positive compartments (VSV^+) were enumerated; the percentage of compartments also positive for NPC1 ($VSV^+/NPC1^+$) or NPC1 plus PLA ($VSV^+/NPC1^+/PLA^+$) were determined. Representative curves out of two independent experiments are shown; averages of pooled cells are displayed ($n \geq 20$ per time point).

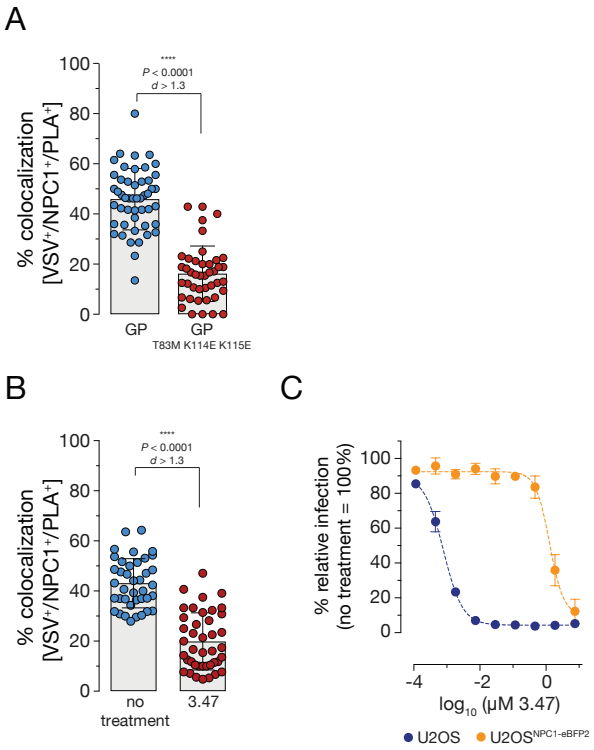

Fig. 2. Proximity ligation is sensitive to perturbations in the GP_{CL}:NPC1 domain C interface. (**A**) VSV mNG-P particles bearing EBOV GP or EBOV $GP^{T83M/K114E/K115E}$ were internalized into $U2OS^{NPC1\text{-}eBFP2}$ cells for 60 min followed by cell fixation, permeabilization and PLA. Cells were analyzed by fluorescence microscopy; data points represent the percentage of $VSV^+/NPC1^+/PLA^+$ compartments per individual cell; bars depict the pooled averages and standard deviations (± SD) for all cells from two independent experiments ($n \geq 40$). An unpaired two-tailed *t*-test was used to compare $VSV^+/NPC1^+/PLA^+$ compartments of cells infected by VSV bearing either EBOV GP or EBOV $GP^{T83M/K114E/K115E}$ (****, $P < 0.0001$). Group means calculated from the percentage of $VSV^+/NPC1^+/PLA^+$ vesicles were compared by Cohen's *d* effect size ($d > 1.3$). (**B**) $U2OS^{NPC1\text{-}eBFP2}$ cells were pre-incubated with the inhibitor 3.47 (1 μM) for 60 min at 37°C, followed by VSV mNG-P EBOV GP uptake for 60 min and PLA. Data points were acquired and analyzed as described in (A). (**C**) After pre-incubation of $U2OS^{NPC1\text{-}eBFP2}$ and wild-type U2OS cells with increasing 3.47 concentrations, cells were infected with VSV mNG-P EBOV GP for 16 h. Infection was measured by automated counting of mNG^+ cells and normalized to infection obtained in the absence of 3.47. Averages ± SD for six technical replicates pooled from two independent experiments are displayed. Data was subjected to nonlinear regression analysis to derive 3.47 concentration at half-maximal inhibition of infection (IC_{50} ± 95% confidence intervals for nonlinear curve fit).

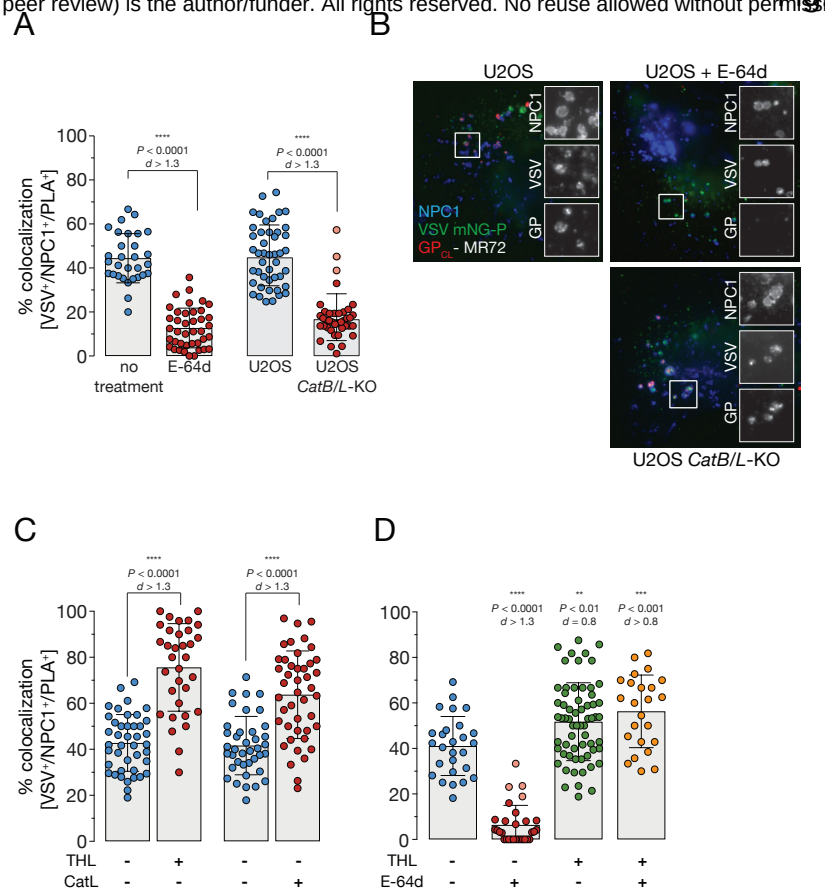

Fig. 3. Detection of GP_{CL}:NPC1 binding by PLA requires endosomal cleavage of GP. (**A**) VSV mNG-P particles bearing EBOV GP were incubated with either $U2OS^{NPC1\text{-}eBFP2}$ cells pre-treated with E-64d (100mM, 6h at 37°C) (left panel), or U2OS *CatB/L*-KO cells ectopically expressing flag-tagged NPC1 (right panel). Cells were fixed following virus incubation (1h at 37°C), permeabilized and subjected to PLA. Data points represent the percentage of $VSV^+/NPC1^+/PLA^+$ compartments per individual cell; bars depict the average ±SD for all data points pooled from two independent experiments ($n \geq 30$). Points with reduced transparency represent values outside of the 10th-90th percentile. An unpaired two-tailed *t*-test was used to compare $VSV^+/NPC1^+/PLA^+$ compartments of wild-type cells with either inhibitor-treated (left) or KO (right) cells infected by EBOV GP-decorated VSV (****, $P < 0.0001$). Group means calculated from the percentage of $VSV^+/NPC1^+/PLA^+$ vesicles were compared by Cohen's *d* effect size. (**B**) Cells described in (A) were exposed to VSV mNG-P EBOV GP uptake for 1h at 37°C. After fixation, viral particles, NPC1 and GP_{CL} were visualized by fluorescence microscopy. Representative images from two independent experiments are shown. (**C**) VSV mNG-P particles bearing EBOV GP were treated *in vitro* with thermolysin (THL) or cathepsin L (CatL), respectively. Viral particles were taken up into $U2OS^{NPC1\text{-}eBFP2}$ cells, followed by fixing of the cells and subjecting them to PLA. Data points represent the percentage of $VSV^+/NPC1^+/PLA^+$ compartments per individual cell; bars depict the average ±SD for all data points pooled from two independent experiments ($n \geq 25$). To compare $VSV^+/NPC1^+/PLA^+$ compartments of cells which endocytosed VSV studded with either uncleaved or THL/CatL- cleaved GP, an unpaired two-tailed *t*-test was used (****, $P < 0.0001$). Cohen's *d* effect size was used to compare the group means calculated from the percentages of $VSV^+/NPC1^+/PLA^+$ vesicles ($d > 1.3$). (**D**) $U2OS^{NPC1\text{-}eBFP2}$ cells were (not) pre-incubated with E-64d (as described in [A]) and VSV mNG-P particles bearing EBOV GP were treated *in vitro* with THL. Following virus internalization into $U2OS^{NPC1\text{-}eBFP2}$, cells were fixed and subjected to PLA. Data points represent the percentage of $VSV^+/NPC1^+/PLA^+$ compartments per individual cell; bars depict the average ±SD for all data points pooled from two independent experiments ($n \geq 25$). Points with reduced transparency represent values outside of the 10th-90th percentile. To compare $VSV^+/NPC1^+/PLA^+$ compartments of E-64d-treated cells with those of untreated cells which endocytosed VSV studded with either uncleaved or THL-cleaved GP, an unpaired two-tailed *t*-test was used (**, $P < 0.01$; ***, $P < 0.001$; ****, $P < 0.0001$). Cohen's *d* effect size was used to compare the group means calculated from the percentages of $VSV^+/NPC1^+/PLA^+$ vesicles.

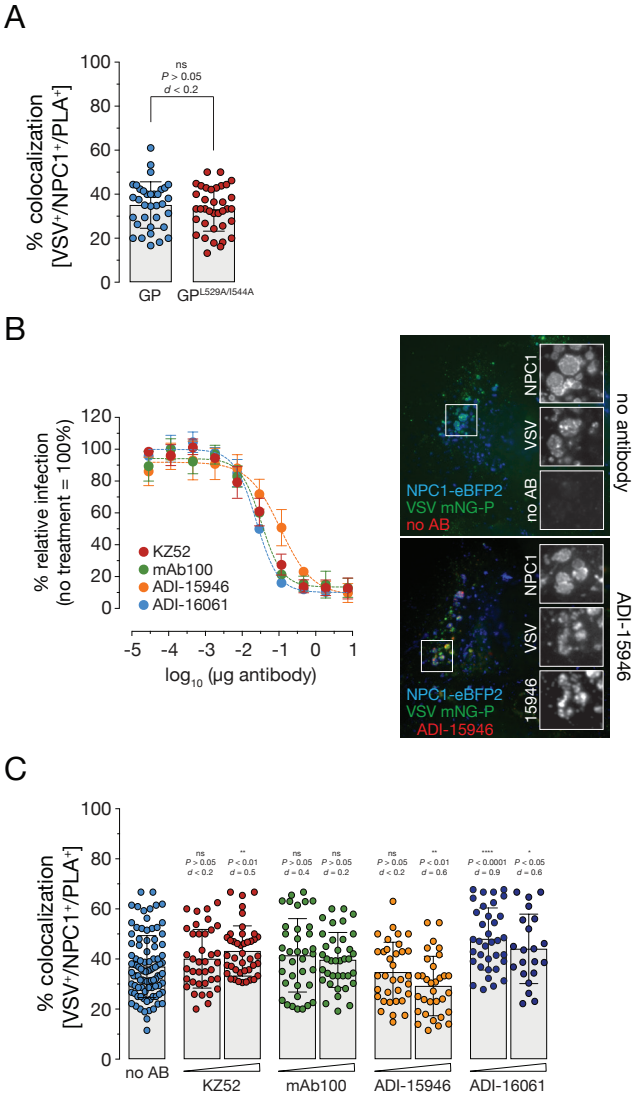

Fig. 4. *In situ* proximity ligation decouples GP_{CL}:NPC1 interaction from post-binding entry steps. (**A**) VSV mNG-P particles bearing EBOV GP or EBOV $GP^{L529A/I544A}$ were internalized into $U2OS^{NPC1\text{-}eBFP2}$ cells for 60 min followed by PLA. Data points represent the percentage of triple positive compartments per individual cell; bars depict the average ±SD for all data points pooled from two independent experiments ($n \geq 37$). Data analyses included an unpaired two-tailed *t*-test to compare $VSV^+/NPC1^+/PLA^+$ vesicles of cells which internalized VSV decorated with wild-type or mutant GP (ns, $P > 0.05$). Cohen's *d* effect size was used to compare the group means calculated from the percentages of $VSV^+/NPC1^+/PLA^+$ compartments. (**B**) ADI-15946 was incubated with VSV EBOV GP particles and exposed to $U2OS^{NPC1\text{-}eBFP2}$ (right panel). After virus uptake for 1h at 37°C, cells were fixed and viral particles, NPC1 and bound antibodies were visualized by fluorescence microscopy. Representative images from two independent experiments are shown. Virions were preincubated with increasing amounts of KZ52, mAb100, ADI-15946 or ADI-16061 and then exposed to $U2OS^{NPC1\text{-}eBFP2}$ cells for 16 h at 37°C (left panel). Number of infected cells was determined by automated counting of mNG^+ cells and normalized to infection obtained in the absence of antibodies. Averages ± SD for six technical replicates pooled from two independent experiments are shown. (**C**) VSV mNG-P EBOV GP virions were complexed with KZ52, mAb100, ADI-15946 or ADI-16061 (50 µg/ml and 100 µg/ml) for 1 h at room temperature. Following internalization into $U2OS^{NPC1\text{-}eBFP2}$, cells were fixed, and subjected to *in situ* PLA. Data points represent the percentage of $VSV^+/NPC1^+/PLA^+$ compartments per individual cell; bars show the average ±SD for all data points pooled from two independent experiments ($n \geq 22$). $VSV^+/NPC1^+/PLA^+$ vesicles were analyzed by unpaired two-tailed *t*-test (ns, $P > 0.05$; *, $P < 0.05$; **, $P < 0.01$; ****, $P < 0.0001$) comparing cells which were exposed to virion-antibody complexes to cells exposed to untreated virus. Group means calculated from the percentage of $VSV^+/NPC1^+/PLA^+$ vesicles were also compared by Cohen's *d* effect size.

Fig. 5

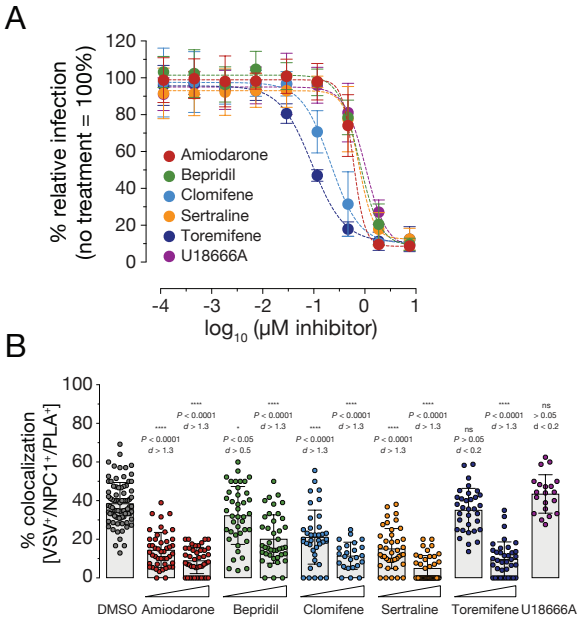

C

drug treatment	virus trafficking	GP_{CL}-NPC1 binding	NPC1 detection	GP_{CL} detection	cholesterol accumulation	NPC1+ LE morphology
no treatment	+++	+++	+++	+++	-	+++
Amiodarone	++	+	+++	++	+++	+
Bepridil	++	++	+++	+++	+	++
Clomifene	++	+	+++	+++	++	+
Sertraline	++	+	+++	+++	+++	+
Toremifene	++	+	+++	++	++	++
U18666A	+++	+++	+++	+++	+++	++

Fig. 5. Small molecule inhibitor-mediated selective interference of GP:NPC1 binding delineated by *in situ* PLA. (**A**) U2OS$^{NPC1\text{-}eBFP2}$ cells were preincubated with increasing concentrations of amiodarone, bepridil, clomifene, sertraline, toremifene, and U18666A, respectively before exposed to VSV mNG-P EBOV GP for 16 h at 37°C. Infection was measured by automated counting of mNG$^+$ cells and normalized to infection obtained in the presence of vehicle only. Averages ± SD for nine to eighteen technical replicates pooled from three to six independent experiments are displayed. (**B**) U2OS$^{NPC1\text{-}eBFP2}$ cells were incubated with amiodarone, bepridil, clomifene, and sertraline, respectively (2 μM or 5 μM, 1 h at 37°C), or toremifene (2 μM or 10 μM, 1 h at 37°C), or U18666A (10 μM, 2 h at 37°C), followed by VSV mNG-P EBOV GP uptake for 1 h. Cells were subjected to *in situ* PLA and analyzed by fluorescence microscopy. The percentage of triple positive VSV$^+$/NPC1$^+$/PLA$^+$ compartments per individual cell is represented by data points; bars show the average ±SD for all data points pooled from two independent experiments ($n \geq 20$). VSV$^+$/NPC1$^+$/PLA$^+$ vesicles were analyzed by unpaired two-tailed *t*-test (ns, $P > 0.05$; *, $P < 0.05$; ****, $P < 0.0001$) comparing inhibitor-exposed to untreated cells. Group means calculated from the percentage of VSV$^+$/NPC1$^+$/PLA$^+$ compartments were also compared by Cohen's *d* effect size. (**C**) Table summarizing results from Fig. 5B and Fig. S6.